Catalysis Today 157 (2010) 236–242

Contents lists available at ScienceDirect

Catalysis Today

journal homepage: www.elsevier.com/locate/cattod

The influence of diffusion phenomena on catalysis: A study at the single particle level using fluorescence microscopy

Gert De Cremer[a], Evelyne Bartholomeeusen[a], Paolo P. Pescarmona[a], Kaifeng Lin[a], Dirk E. De Vos[a], Johan Hofkens[b], Maarten B.J. Roeffaers[b], Bert F. Sels[a,*]

[a] Department of Microbial and Molecular Systems, Katholieke Universiteit Leuven, Kasteelpark Arenberg 23, B-3001 Heverlee, Belgium
[b] Department of Chemistry, Katholieke Universiteit Leuven, Celestijnenlaan 200F, B-3001 Heverlee, Belgium

ARTICLE INFO

Keywords:
Fluorescence microscopy
Diffusion limitation
Epoxidation
Ti-MCM-41
Thiele modulus

ABSTRACT

Mass transfer phenomena are known to play a crucial rule in porous heterogeneous catalysts. When intraparticle diffusion is too slow to provide a sufficient flux of reactants to the inner parts of the catalyst particles, substrate depletion occurs and only the outer parts of the particles are efficiently used for catalysis. Quantifying the degree of intraparticle diffusion limitation by means of the Thiele modulus and the related effectiveness factor remains a big challenge. Only few techniques combine the necessary spatial resolution and sensitivity to measure *in situ* the concentration profiles of organic products and/or reagents inside the catalytic particles. In this contribution a brief overview is given of *in situ* techniques that allow such space-resolved activity profiling at the single particle level and their strengths and weaknesses are highlighted. The superior sensitivity of fluorescence microscopy is exploited to study the effects of mass transfer limitations on the overall catalytic efficiency *in a spatially resolved fashion*. The epoxidation of bulky substrates over mesoporous Ti-MCM-41 was chosen as a model case. It is shown how individual reaction events inside the Ti-MCM-41 particles are visualized and localized and how the obtained reactivity maps yield direct information on the Thiele modulus and effectiveness factor of this specific intraparticle diffusion limited catalytic process. Moreover, a value for the intraparticle diffusion constant and the intrinsic rate constant of the catalytic reaction could be estimated based on the data obtained by one *in situ* experiment. The presented method is versatile and applicable to a variety of catalytic systems, provided that a suitable fluorogenic probe molecule is used, which preferably is detectable at the single molecule level after catalytic conversion.

1. Introduction

Heterogeneous catalysts offer unique opportunities for sustainable chemical processes, thanks to the ease of separation and recycling of the catalyst from the reaction mixture resulting in cleaner waste streams. In heterogeneous catalysis the reaction takes place at the interface between the solid catalyst and the liquid or gas phase where the reactants are located. Therefore, it is crucial to maximize the contact area between the catalyst and the reaction medium. This can be achieved by using highly porous catalysts, displaying very large accessible surface areas. However, the increased surface area in nanoporous materials is often counteracted by the slower diffusion of reactants and products through the catalytic material. To evaluate how the reaction rate is influenced by the reactant supply to the inner parts of the particles, a detailed understanding of the involved diffusion processes in relation with the catalytic rate is essential. When intraparticle diffusion of the reactants to the catalyst center is the rate determining step in the process, the catalyst is not only used inefficiently, but also, the longer residence times of the formed product molecules may give rise to secondary reactions, resulting in a decreased selectivity. The latter for instance can be problematic in the partial oxidation of hydrocarbons [1,2].

Intraparticle diffusion limitations can often be overcome by decreasing the particle size. As such, measuring the catalytic rate as a function of particle size can be used to check whether or not the reaction is under intraparticle diffusion control. However, decreasing the particle size might induce different particle morphologies or the overexposure of certain crystallographic planes and hence alter the overall pore accessibility. For instance, in ZSM-5 crystals the crystal morphology is very sensitive towards the synthesis procedure and thus also towards the particle size [3,4]. Therefore it is not always straightforward to directly relate variations in activity to particle size. A more quantitative approach to evaluate the influence of intraparticle diffusion on the overall catalytic process was

* Corresponding author.
E-mail addresses: maarten.roeffaers@chem.kuleuven.be (M.B.J. Roeffaers), bert.sels@biw.kuleuven.be (B.F. Sels).

0920-5861/$ – see front matter © 2010 Elsevier B.V. All rights reserved.
doi:10.1016/j.cattod.2010.04.035

elaborated by Thiele and later by Wheeler [5–7]. By constructing the mass balance for the reactant in a spherical catalyst particle with radius r_1 and using as boundary conditions $c = c_1$ at $r = r_1$ and c is finite at $r = 0$, the concentration profile inside the particle could be derived (see Eq. (1)).

$$c(r) = c_1 \cdot \frac{r_1}{r} \cdot \frac{\sinh(m \cdot r)}{\sinh(m \cdot r_1)} = c_1 \cdot \frac{r_1}{r} \cdot \frac{e^{m \cdot r} - (1/e^{m \cdot r})}{e^{m \cdot r_1} - (1/e^{m \cdot r_1})} \text{ with}$$

$$m = \sqrt{\frac{k}{D_{eff}}} \quad (1)$$

From Eq. (1) it can be seen that m^{-1} represents the characteristic distance over which the concentration profile decays. Thus, in the case of intraparticle diffusion limitation, when m^{-1} is small compared to the particle radius r_1, the equation can be simplified to:

$$c(r) = c_1 \cdot e^{m \cdot (r - r_1)} \text{ for } r \approx r_1 \quad (2)$$

The dimensionless (modified) Thiele modulus (ϕ) is defined as the ratio between the characteristic particle size (volume V_p over surface area S_p) and the distance of concentration decay m^{-1}, and is a direct measure of intraparticle diffusion limitation (Eq. (3)).

$$\phi = \frac{V_p}{S_p} \cdot m = \frac{V_p}{S_p} \cdot \sqrt{\frac{k}{D_{eff}}} \quad (3)$$

For ϕ larger than 1, intraparticle diffusion becomes rate determining. The dimensionless effectiveness factor η is related to ϕ. η is defined as the ratio of the real reaction rate over the theoretical reaction rate when the concentration along the whole particle would equal the external concentration.

$$\eta = \frac{1}{\phi} \cdot \left[\coth(3 \cdot \phi) - \frac{1}{3 \cdot \phi} \right] \quad (4)$$

For high Thiele moduli, η approaches $1/\phi$ while at low Thiele moduli η approaches 1. This theory simply relates basic parameters in order to quantify the influence of diffusion limitations on the catalytic performance of a porous material. Nevertheless it remains extremely hard to get experimental access to these parameters, *viz*. the effective diffusivity D_{eff} and the intrinsic rate constant k. Generally the presence of intraparticle diffusion limitations is identified through indirect measurements, such as measuring the apparent activation energy as a function of temperature or measuring the dependency between particle size and activity [7]. For a real quantification of the Thiele-Wheeler parameters, exact values for the intraparticle diffusion coefficient and rate constant must be obtained in relevant conditions, which is a tedious task. *In situ* NMR-based techniques such as Pulsed Field Gradient (PFG) NMR or Pulsed Gradient Spin Echo (PGSE) NMR can be applied to obtain intraparticle diffusion coefficients of hydrogen-containing compounds such as hydrocarbons in reaction conditions [8,9]. However, the range of measurable diffusion constants with this technique is generally limited to D values larger than 10^{-14} m^2/s. Moreover, PFG NMR measures the diffusivities only at the microscale, over distances much smaller than the crystallite size. Therefore particular effects in macroscopic crystal properties such as transport barriers are not taken into account [10].

In this contribution we present a new, generic approach for direct visualization and quantification of the intraparticle diffusion limitations and the related Thiele–Wheeler parameters, via space-resolved activity profiling inside individual catalytic particles. After a concise overview of techniques for direct space-resolved activity profiling, we will elaborate this approach for the specific example of activity profiling with the aid of high-resolution single molecule fluorescence microscopy on individual Ti-MCM-41 epoxidation catalysts using a profluorescent model reagent. This catalyst is often used for the epoxidation of bulky substrates, which cannot enter the smaller pores of the more performing TS-1 catalyst [11,12]. Recently it was demonstrated that the particle size has a strong influence on the activity and selectivity of the epoxidation reaction [13,14]. It was therefore reasoned that the common micrometer-sized Ti-MCM-41 particles are not optimally used due to intraparticle diffusion limitations.

2. Direct visualization of mass transfer phenomena during catalysis: space-resolved reaction profiling

A direct quantification of intraparticle diffusion limitations through the Thiele modulus is possible since its value is only determined by the particle radius and the characteristic distance over which reaction takes place inside the particle (see m-value in Eqs. (1) and (2)). The latter can be effectively probed by any space-resolved technique that can selectively monitor product formation *in situ* at the single particle level [15]. However, in practice many limitations arise. For instance NMR-based MRI imaging has a limited spatial resolution of about 100 μm, and can therefore only be used for catalyst pellets, which are in fact assemblies of individual catalytic particles [16,17]. A better spatial resolution of 5–20 μm in the *xy*-plane is provided by (ATR) IR microscopy, a technique that also yields detailed chemical information on the probed molecule via its vibrational fingerprint [18,19]: however the lack of *Z*-resolution can be a limiting factor for its application on product formation inside individual particles. Microscopy methods using light of lower wavelengths, for instance UV–vis microscopy, logically yield better resolution; however, this resolution is limited to the *xy*-plane [20]. A true diffraction-limited 3D resolution using visible light can be achieved by confocal Raman microscopy [21–23]. Although all these techniques are promising for use in space-resolved activity profiling at the single catalyst level, there is still a big hurdle that must be overcome: their limited sensitivity. In real steady-state catalytic processes the products quickly diffuse out of the particles and thus at each moment only a small amount of product molecules is present inside one catalytic particle. In order to monitor product formation in such situations, the techniques mentioned so far will often lack sensitivity and are therefore not always suitable for investigating catalysis and related mass transfer phenomena at the single particle level. Here, *in situ* fluorescence microscopy provides a solution. The extremely high sensitivity, down to the single molecule level, allows the detection of very limited amounts of fluorophores, while the diffraction-limited spatial resolution is typically in the order of a few hundred nanometers. A true 3D resolution is achievable allowing to make resolved optical sections throughout catalytic particles. Recently, several strategies were even developed to circumvent the diffraction limit, yielding nanometer resolution in the *xy*-plane [24–30]. Aside from numerous fluorescence microscopy-based studies on diffusion in porous media [31–35], it was recently demonstrated that this technique can be a valuable tool for monitoring catalysis as well [36–45]. However, when it comes to catalysis inside porous media, so far only a few examples have been reported. In these studies the fluorescent product molecules were trapped in the inner pore volume [36,42,46,47]. As a result, the accumulation of these products is easy to monitor with diffraction-limited resolution, but such non-steady-state conditions are not always relevant for real catalytic processes. This contribution therefore shows how single molecule fluorescence microscopy can yield high-resolution activity profiles inside a porous catalyst in steady-state conditions and this beyond the diffraction limit. The obtained activity profiles yield direct information on the overall catalytic process including mass transfer phenomena. By only one experiment, the Thiele modulus and effectiveness factor can be directly deduced and intraparticle diffusion coefficients as well as rate constants of

the catalytic activity can be calculated for liquid phase catalytic systems.

3. Materials and methods

3.1. Synthesis of Ti-MCM-41

The general synthesis scheme of the Ti-MCM-41 particles is described in detail elsewhere [13,14]. The material was prepared from a synthesis mixture consisting of an aqueous solution of cetyltrimethylammonium bromide (CTAB), tetraethyl orthosilicate (TEOS), titanium (IV) isopropoxide (TIP) and an aqueous ammonia solution. The molar ratio of H_2O/NH_3/CTAB/TEOS/TIP was 62/3.3/0.1/1/0.025. The obtained gel was heated at 100 °C in an autoclave for 48 h under static conditions, after which the solid was centrifuged, washed with distilled water, dried at 60 °C, and calcined in air at 550 °C for 6 h (with a heating rate of 1 °C/min). This way Ti-MCM-41 with an average particle size of ±3 μm was obtained. A profound characterization of this material has been published elsewhere [14]. From N_2-adsorption measurements a uniform pore size of about 2.7 nm without the presence of larger void spaces between the mesoporous domains in the MCM-41 particle was evidenced. X-ray diffractograms illustrated the high degree of ordering in this material, while from UV–vis spectroscopy the absence of TiO_2 in the anatase phase was proven [14].

3.2. Synthesis of phenylbutadienyl-substituted boron dipyrromethene difluoride (PBD-bodipy)

The synthesis of the PBD-bodipy probe is described in detail elsewhere [48]. Before the measurements an additional purification is performed by silica chromatography with pure dichloromethane as eluent. The first fraction (RF = 0.95) is the desired product.

3.3. Fluorescence microscopy measurements

The wide field fluorescence microscope consists of an inverted microscope (IX-71, Olympus) in combination with a 100×, 1.3 NA oil immersion objective lens and a highly sensitive cooled Electron Multiplying-CCD (cascade 512B, Princeton Instruments Inc.). The excitation source is a 488 nm Ar^+ laser (Stabilite 2017, Spectra-Physics), operating at 200 mW, which is circularly polarized, expanded and focused onto the back focal plane of the objective. Emission is collected by the same objective, split from the excitation beam by a dichroic mirror, spectrally cleaned by a long pass 500 nm and a bandpass 509–547 nm filter to remove unwanted red emission from the unreacted PBD-bodipy substrate, and imaged by the CCD with a frame rate of 10 Hz. The image was expanded 3.3 times before entering the CCD, resulting in a field of view of 24.6 μm × 24.6 μm.

The sample is prepared by spin coating a suspension of the Ti-MCM-41 particles in *n*-butanol onto a clean cover glass. These cover glasses are subsequently mounted in a sample holder that allows for the addition of liquids. After addition of solvent (*n*-butanol, spectroscopic grade and vacuum distilled) and the reagents, *tert*-butylhydroperoxide (TBHP) and PBD-bodipy, the sample was mounted on the microscope. Reactions are performed at room temperature.

3.4. XPS measurements

XPS measurements on the Ti-MCM-41 particles are performed using a S-Probe Monochromatized XPS spectrometer of Surface Science Instruments (VG), equipped with a Al Kα X-ray source (1486.6 eV monochromatic). The take-off angle was $\theta = 45°$. The sample was mounted in a vacuum chamber at a pressure of 2×10^{-9} mbar. The analysis surface was approximately 250 μm × 1000 μm.

3.5. Measuring pore accessibility

The accessibility of the Ti-MCM-41 pores for the PBD-bodipy probe was measured by immersing the particles in a concentrated PBD-bodipy solution (±1 mM) in *n*-butanol. Subsequently the particles were washed once in *n*-butanol and spin coated on a clean cover glass. 3D imaging of the fluorescence intensity distribution inside the particles is performed on a confocal laser scanning microscope (Olympus Fluoview 500) under 543 nm excitation. The pinhole was set to 100 μm to ensure a reasonable *Z*-resolution.

4. Results and discussion

To probe the epoxidation activity of an individual Ti-MCM-41 particle with *tert*-butyl hydroperoxide (TBHP) as oxidant, a phenylbutadienyl-substituted boron dipyrromethene difluoride (PBD-bodipy) is applied. Upon oxidation of one of the double bonds in the butadienyl bridge (Fig. 1a) the fluorescence color shifts from red to green-yellow. The reactivity of this probe towards epoxidation is examined at the bulk level. Fig. 1b shows the absorption and emission spectra of a reaction mixture of the PBD-bodipy (10 mM) probe and *tert*-butyl hydroperoxide (TBHP; 10 mM) in *n*-butanol in the presence 5 mg of the Ti-MCM-41 catalyst, measured at low to intermediate conversions (after 10 h stirring at 60 °C), to minimize the formation of the double epoxide product P_3. Two blue-shifted

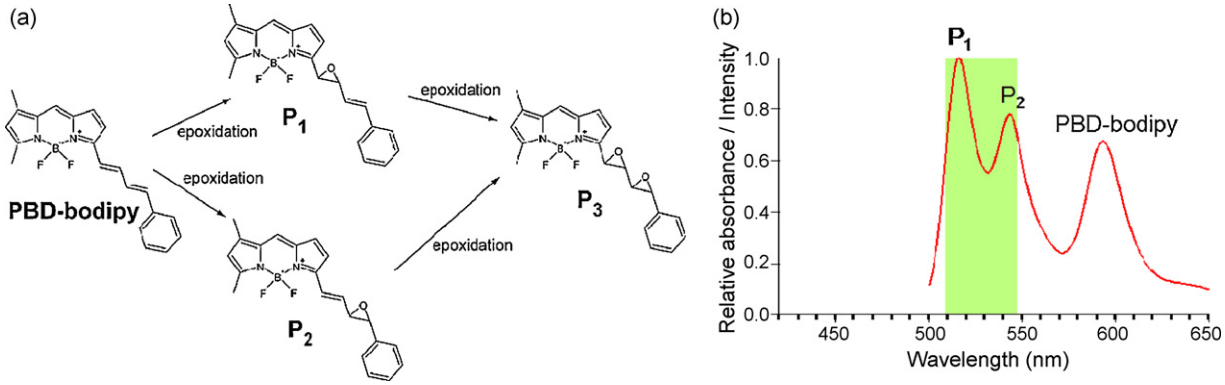

Fig. 1. Bulk fluorescence properties of the PBD-bodipy (10 mM) probe and its epoxidation products (P_1, P_2 and P_3) in *n*-butanol upon 488 nm excitation. In the presence of *tert*-butyl hydroperoxide (TBHP; 10 mM) and Ti-MCM-41 catalysts (5 mg) the emission spectrum shifts from red to greenish-yellow due to the formation of the products P_1 and P_2. The spectrum is taken at low (<5%) conversion, thus the amount of formed P_3 is negligible. The green rectangle indicates the part of the spectrum that is collected in the microscopic single molecule experiments. (For interpretation of the references to color in this figure legend, the reader is referred to the web version of the article.)

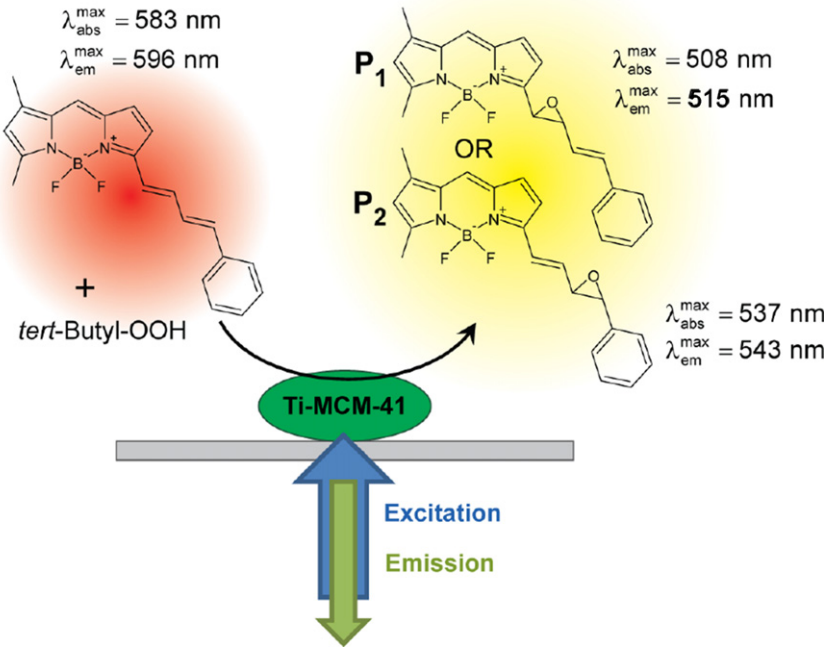

Fig. 2. Scheme of the experimental setup. Upon epoxidation of the PBD-bodipy probe in the Ti-MCM-41 catalyst a yellow fluorescent product is formed, the emission of which is collected upon excitation by a 488 nm laser. (For interpretation of the references to color in this figure legend, the reader is referred to the web version of the article.)

bands are observed. The first band has excitation and emission maxima around 508 and 515 nm respectively and is assigned to product 1 (P_1), while the second band, having excitation and emission maxima around 537 and 543 nm respectively is assigned to product 2 (P_2).

For the microscopy measurements (see Fig. 2 for a schematic overview) the catalytic particles are deposited on a glass slide by spin coating from a suspension in *n*-butanol. The slide is then introduced in the measurement cell. After addition of the reaction mixture (0.5 μM PBD-bodipy and 35 mM TBHP in *n*-butanol) fluorescence images were recorded at a rate of 10 frames/s. The large excess of TBHP assures that the reaction kinetics can be considered to be pseudo-first order with respect to the PBD-bodipy concentration. It is assumed that the rate-limiting step in the catalytic reaction is the oxygen transfer from the Ti-peroxo complex, formed from the Ti sites in the Ti-MCM-41 particles by TBHP, to the PBD-bodipy probe.

When the focal plane of the setup was moved to the middle of an individual catalytic particle, fluorescent flashes with a diffraction-limited size were observed at a rate of 0.1 till 1.5 spots/s (Fig. 3a–d). Every fluorescent spot corresponds to the formation of a single product molecule (P_1 or P_2). The position of every reaction event inside the catalytic particle can be determined with an accuracy below the diffraction limit, just by fitting the intensity profile of the emissive spot by a 2D Gaussian in order to find its center-of-mass. Details of the turnover-based "high-resolution" strategy are published elsewhere [24,49]. By accumulating a sufficient number of frames over time and by localizing all reaction events, a map of the Ti-MCM-41 reactivity can be constructed (Fig. 3e). In this case, localization accuracies between 10 and 15 nm were reproducibly obtained. This map directly reveals which fraction of the particles is efficiently used in catalysis and can thus be related to the Thiele modulus (ϕ) and the effectiveness parameter (η).

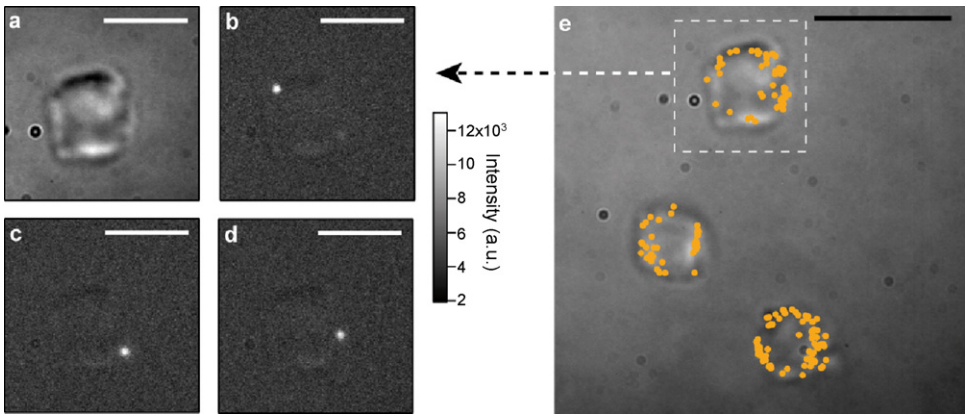

Fig. 3. (a) Transmission image of an individual Ti-MCM-41 particle. (b–d) Three representative examples of fluorescent bursts due to the formation of a single product molecule in the Ti-MCM-41 catalyzed epoxidation of the PBD-bodipy probe. The white scale bars in panels a–d represent a distance of 3 μm. (e) Transmission image of three Ti-MCM-41 particles on which the positions where reactions were observed over a time span of 140 s are highlighted by a yellow mark. The black scale bar represents a distance of 5 μm. (For interpretation of the references to color in this figure legend, the reader is referred to the web version of the article.)

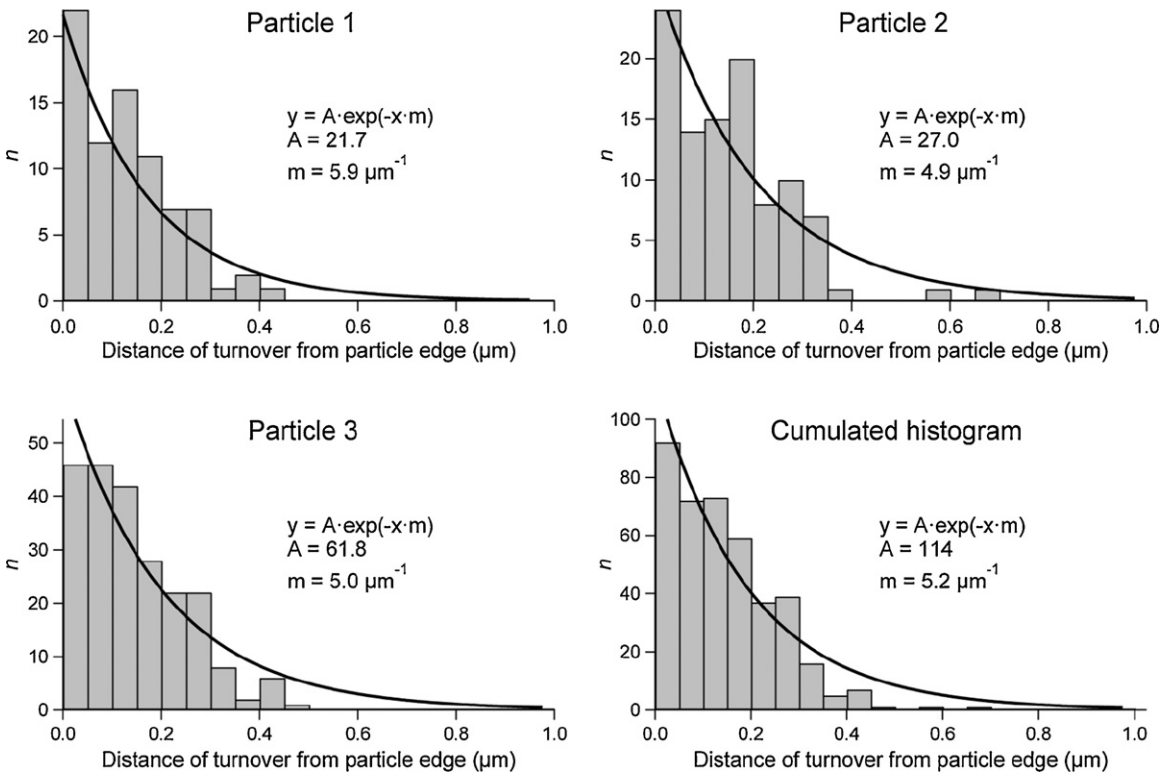

Fig. 4. Histograms of the distances between the turnover's locations and the particle's edge for three representative Ti-MCM-41 particles with a radius of ±1.5 μm. The fourth, cumulated histogram contains the distances for the three particles together. The solid line represents a mono-exponential fit to the data.

In order to determine the width of the active rim of the Ti-MCM-41 particles, the distances between the location of every turnover and the particle's edge were measured for a few representative Ti-MCM-41 particles. The histograms of these distances are shown in Fig. 4. A mono-exponential fit to these histograms directly yields the m-values for the catalytic process in the corresponding particles. These m-values vary from 4.9 to 5.9 μm^{-1} for the three examples in Fig. 4, corresponding to characteristic widths of the active rim ($1/m$) of 170–205 nm.

The Thiele moduli (Eq. (3)) and effectiveness factors (Eq. (4)) for these particles are summarized in Table 1 and are in the range of 2–3 and 0.30–0.42, respectively. These values quantitatively demonstrate the presence of considerable intraparticle diffusion limitation in this catalytic system. One simple experiment thus yields all the necessary information to estimate the Thiele modulus and the effectiveness factor directly. Moreover, the intraparticle effective diffusion coefficient (D_{eff}) can be calculated from these experimental data. The reagent flux inside the particle at the outer surface equals the net influx of reagents from the bulk solution into the particles and thus in steady-state conditions this must equal the total observed rate inside the particles ($rate_{total}$).

$$J_{\text{intraparticle}}(r_1) \cdot A = D_{eff} \cdot \left(\frac{\partial c}{\partial r}\right)_{r=r_1} \cdot 4 \cdot \pi \cdot r_1^2 = rate_{total} \tag{5}$$

Turnover spots were recorded by moving the focal plane of the microscope to the middle of the particles and due to rejection of the more blurry out-of-focus turnovers by the analysis software only turnovers occurring over a Z-distance of a few hundred micrometer around the focal plane are seen as bright fluorescent spots. The outer rim in this focal volume contributes for approximately 10% to the total rim volume. As for the three particles highlighted in Fig. 3 about 0.8–1.3 turnovers/s were observed in the focal volume, the total rate of the individual particles particle lies in the range of $1.3–2.1 \times 10^{-23}$ mol/s per particle (see Table 1). Combining Eqs. (2) and (5) results in Eq. (6):

$$D_{eff} = \frac{rate_{total}}{c_1 \cdot m \cdot 4 \cdot \pi \cdot r_1^2} \tag{6}$$

The obtained D_{eff} is in the order of magnitude of 10^{-16} to 10^{-17} m^2/s (see Table 1). Subsequently the rate constant k (which is

Table 1
Overview of intraparticle diffusion versus activity characteristics for three representative individual Ti-MCM-41 particles. The values are obtained from the measured intraparticle activity profiles.

	r (μm)	$1/m$ (nm)	$Rate_{total}$ (mol/s)	ϕ	η	D_{eff} (m^2/s)	k' (s^{-1})
Particle 1	1.5	170	1.3×10^{-23}	3.0	0.30	1.6×10^{-16}	5.4×10^{-3}
Particle 2	1.5	200	2.1×10^{-23}	2.5	0.35	3.0×10^{-16}	7.4×10^{-3}
Particle 3	1.2	205	1.3×10^{-23}	2.0	0.42	2.9×10^{-16}	7.0×10^{-3}
Average	1.4	192[a]	1.6×10^{-23}	2.4[b]	0.36[b]	2.5×10^{-16}[b]	6.8×10^{-3}[b]

[a] Value obtained from fitting the cumulated histogram.
[b] Values obtained from calculations based on $\langle r \rangle$, and $\langle rate_{total} \rangle$.

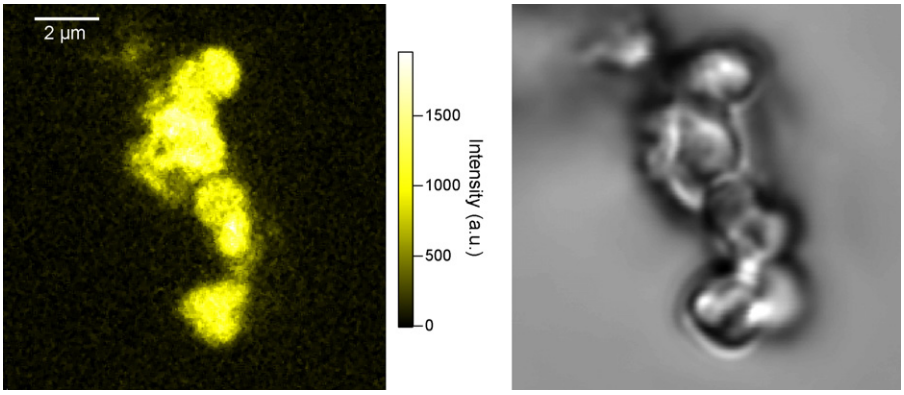

Fig. 5. Adsorption of excess PBD-bodipy in Ti-MCM-41 particles in the absence of oxidant. The left image shows the fluorescence intensity upon 532 nm excitation focused in the middle of the Ti-MCM-41 particles, seen through a confocal fluorescence microscope. The right image shows a transmission image of the same region.

in this case a pseudo-first order rate constant k') can be estimated since m and D_{eff} are known:

$$k' = m^2 \cdot D_{eff} \tag{7}$$

This pseudo-first order rate constant varies from 5 to $7.5 \times 10^{-3}\ s^{-1}$ for the three Ti-MCM-41 particles in these reaction conditions (see Table 1).

Thus, parameters such as the intraparticle diffusion constant D_{eff} and the rate constant k of the catalyzed reaction, which are extremely hard to obtain by any other method, can also be calculated based on the results from this microscopic *in situ* measurement.

Finally, some control experiments are performed to exclude other effects that might induce rim activity in Ti-MCM-41 catalysis. Firstly, to confirm that the active Ti sites are homogeneously distributed throughout the Ti-MCM-41 particles, XPS measurements were performed to measure the surface concentration of Ti. A surface Ti/Si molar ratio of 1/110 was found, which is in line with the average Ti/Si molar ratio obtained by bulk chemical analysis. It can thus be concluded that there is no significant enrichment of Ti towards the particle's outer rim.

Secondly, the absence of physical pore blocking is checked. In the absence of the TBHP oxidant, the PBD-bodipy molecules can reach the inner parts of the Ti-MCM-41 particles as evidenced by confocal fluorescence microscopy (Fig. 5). Here, a 532 nm laser was used as an excitation source to visualize the red fluorescence from the PBD-bodipy molecule itself, after immersion of the Ti-MCM-41 particles in a concentrated PBD-bodipy solution. These results exclude the possibility that there is a physical barrier that prevents the PBD-bodipy probe from reaching the inner parts of the Ti-MCM-41 pore system.

As the microscopic experiments are performed in non-stirred conditions, it is reasonable to assume that the particles are surrounded by an infinitely thick solvent film. To exclude the possibility that film diffusion limitations are present in the reaction solution, the concentration gradient of the BPD-bodipy probe, Δc_{film}, from the bulk solution (c_{bulk} = 0.5 μM) towards the particle's outer rim (at $r = r_1$) is calculated by applying the mass balance over this volume (Eq. (8)):

$$\Delta c_{film} = c_{bulk} - c(r_1) = \frac{rate_{total}}{D_{film} \cdot 4 \cdot \pi \cdot r_1} \tag{8}$$

In Eq. (8), D_{film} represents the diffusion constant in the bulk solution (film), which can be estimated to be approximately $10^{-10}\ m^2/s$ [50]. The total rate of product formation ($rate_{total}$) of one particle is about 2×10^{-23} mol/s for the most active particles. This yields a concentration gradient of about 10 pM, which is negligible with respect to the total bulk concentration. There is thus no significant substrate depletion towards the catalytic particles in the microscope experiments.

5. Conclusion and outlook

The presented experimental results prove that (single molecule) fluorescence microscopy is a valuable tool for constructing reactivity profiles inside individual catalytic particles at (sub)micrometer length scales. The extreme detection sensitivity even allows to do this for particles with relatively low activity and in which the fluorescent products do not accumulate. The technique is applicable to condensed phase catalysis under ambient conditions, which, together with the spatio-temporal resolution, makes it a unique tool in catalytic research. This is illustrated here for the Ti-MCM-41 epoxidation of olefinic substrates at the single turnover level. The obtained reactivity maps contain information on mass transfer limitation in the overall catalytic process, which can be directly measured and translated into the Thiele modulus and the effectiveness factor. In addition, the intraparticle diffusion coefficient and the rate constant of the catalyzed reaction can be calculated at the level of individual particles from the obtained results without additional experiments. The presented approach is generic and therefore valuable for catalytic research in general.

As new strategies are constantly arising for pushing down the spatial resolution more and more below the diffraction limit, even in the *Z*-dimension [51], the suggested scheme will become applicable to ever smaller-sized particles. In a very optimistic scenario, mass transfer phenomena and catalysis may even be studied at the level of individual pores [33]. The ease of combining fluorescence microscopy with Raman microscopy further provides interesting perspectives for investigating the influence of intraparticle heat transfer on the overall catalytic process in the case of non-isothermal reactions. Indeed, the intensity ratio between Stokes and anti-Stokes signals can be used for space-resolved thermometry. Taking into account the current success as well as the future perspectives that still have to be explored, a bright future can be expected for fluorescence microscopy in catalytic research.

Acknowledgements

G.D.C. and M.B.J.R. thank the FWO (Fonds voor Wetenschappelijk Onderzoek) for fellowships. This work was performed within the framework of the IAP-VI program "Functional Supramolecular Systems" of the Belgian Federal government and of GOA-2/01. We also gratefully acknowledge financial support from a long-term structural funding "Methusalem" by the Flemish government and from K.U. Leuven. Peter Dedecker is thanked for help with the analysis routine.

References

[1] T.H. Kim, B. Ramachandra, J.S. Choi, M.B. Saidutta, K.Y. Choo, S.D. Song, Y.W. Rhee, Catal. Lett. 98 (2004) 161.
[2] J. Zhang, X. Liu, R. Blume, A.H. Zhang, R. Schlogl, D.S. Su, Science 322 (2008) 73.
[3] J.H. Koegler, H. van Bekkum, J.C. Jansen, Zeolites 19 (1997) 262.
[4] M.B.J. Roeffaers, R. Ameloot, M. Baruah, H. Uji-i, M. Bulut, G. De Cremer, U. Muller, P.A. Jacobs, J. Hofkens, B.F. Sels, D.E. De Vos, J. Am. Chem. Soc. 130 (2008) 5763.
[5] A. Wheeler, Adv. Catalysis, Vol.3, Academic Press, 1951, pp. 249.
[6] E.W. Thiele, Ind. Eng. Chem. 31 (1939) 916.
[7] J.M. Thomas, W.J. Thomas, Principles and practice of heterogeneous catalysis, VCH:Weinheim, Weinheim, 1997.
[8] H.B. Schwarz, S. Ernst, J. Karger, B. Knorr, G. Seiffert, R.Q. Snurr, B. Staudte, J. Weitkamp, J. Catal. 167 (1997) 248.
[9] R.Q. Snurr, A. Hagen, H. Ernst, H.B. Schwarz, S. Ernst, J. Weitkamp, J. Karger, J. Catal. 163 (1996) 130.
[10] O. Geier, S. Vasenkov, E. Lehmann, J. Karger, U. Schemmert, R.A. Rakoczy, J. Weitkamp, J. Phys. Chem. B 105 (2001) 10217.
[11] M. Taramasso, G. Perego, B. Notari, US Patent 4,410,501, US Patent 4,410,501 (1983).
[12] A.J.H.P. Vanderpol, A.J. Verduyn, J.H.C. Vanhooff, Appl. Catal. A 92 (1992) 113.
[13] K.F. Lin, P.P. Pescarmona, K. Houthoofd, D.D. Liang, G. Van Tendeloo, P.A. Jacobs, J. Catal. 263 (2009) 75.
[14] K.F. Lin, P.P. Pescarmona, H. Vandepitte, D. Liang, G. Van Tendeloo, P.A. Jacobs, J. Catal. 254 (2008) 64.
[15] A. Urakawa, A. Baiker, Topics Catal. 52 (2009) 1312.
[16] J.A. Bergwerff, A.A. Lysova, L.E. Alonso, I.V. Koptyug, B.M. Weckhuysen, Angew. Chem., Int. Ed. 46 (2007) 7224.
[17] I.V. Koptyug, A.A. Lysova, R.Z. Sagdeev, V.N. Parmon, Catal. Today 126 (2007) 37.
[18] R. Morschl, J. Bolten, A. Bonnefont, K. Krischer, J. Phys. Chem. C 112 (2008) 9548.
[19] E. Stavitski, M.H.F. Kox, I. Swart, F.M.F. de Groot, B.M. Weckhuysen, Angew. Chem., Int. Ed. 47 (2008) 3543.
[20] M.H.F. Kox, E. Stavitski, B.M. Weckhuysen, Angew. Chem., Int. Ed. 46 (2007) 3652.
[21] I.E. Wachs, Catal. Today 27 (1996) 437.
[22] J.A. Bergwerff, L.G.A. van de Water, T. Visser, P. de Peinder, B.R.G. Leliveld, K.P. de Jong, B.M. Weckhuysen, Chem. Eur. J. 11 (2005) 4592.
[23] A. Urakawa, N. Maeda, A. Baiker, Angew. Chem., Int. Ed. 47 (2008) 9256.
[24] M.B.J. Roeffaers, G. De Cremer, J. Libeert, R. Ameloot, P. Dedecker, A.J. Bons, M. Bückins, J.A. Martens, B.F. Sels, D.E. De Vos, J. Hofkens, Angew. Chem., Int. Ed. 48 (2009) 9285.
[25] E. Betzig, G.H. Patterson, R. Sougrat, O.W. Lindwasser, S. Olenych, J.S. Bonifacino, M.W. Davidson, J. Lippincott-Schwartz, H.F. Hess, Science 313 (2006) 1642.
[26] P. Dedecker, C. Flors, J.I. Hotta, H. Uji-I, J. Hofkens, Angew. Chem., Int. Ed. 46 (2007) 8330.
[27] S.W. Hell, Science 316 (2007) 1153.
[28] S.T. Hess, T.P.K. Girirajan, M.D. Mason, Biophys. J. 91 (2006) 4258.
[29] M.J. Rust, M. Bates, X.W. Zhuang, Nat. Methods 3 (2006) 793.
[30] P. Tinnefeld, M. Sauer, Angew. Chem., Int. Ed. 44 (2005) 2642.
[31] M.B.J. Roeffaers, B.F. Sels, D. Loos, C. Kohl, K. Mullen, P.A. Jacobs, J. Hofkens, D.E. De Vos, Chemphyschem 6 (2005) 2295.
[32] C. Hellriegel, J. Kirstein, C. Brauchle, New J. Phys. 7 (2005).
[33] A. Zurner, J. Kirstein, M. Doblinger, C. Brauchle, T. Bein, Nature 450 (2007) 705.
[34] S. Ito, S. Fukuya, T. Kusumi, Y. Ishibashi, H. Miyasaka, Y. Goto, M. Ikai, T. Tani, S. Inagaki, J. Phys. Chem. C 113 (2009) 11884.
[35] S.M. Mahurin, S. Dai, M.D. Barnes, J. Phys. Chem. B 107 (2003) 13336.
[36] M.B.J. Roeffaers, J. Hofkens, G. De Cremer, F.C. De Schryver, P.A. Jacobs, D.E. De Vos, B.E. Sels, Catal. Today 126 (2007) 44.
[37] M.B.J. Roeffaers, B.F. Sels, H. Uji-i, F.C. De Schryver, P.A. Jacobs, D.E. De Vos, J. Hofkens, Nature 439 (2006) 572.
[38] W.L. Xu, J.S. Kong, Y.T.E. Yeh, P. Chen, Nat. Mater. 7 (2008) 992.
[39] K. Blank, G. De Cremer, J. Hofkens, Biotechnol. J. 4 (2009) 465.
[40] G. De Cremer, M.B.J. Roeffaers, M. Baruah, M. Sliwa, B.F. Sels, J. Hofkens, D.E. De Vos, J. Am. Chem. Soc. 129 (2007) 15458.
[41] B.P. English, W. Min, A.M. van Oijen, K.T. Lee, G.B. Luo, H.Y. Sun, B.J. Cherayil, S.C. Kou, X.S. Xie, Nat. Chem. Biol. 2 (2006) 87.
[42] M.H.F. Kox, E. Stavitski, J.C. Groen, J. Perez-Ramirez, F. Kapteijn, B.M. Weckhuysen, Chem. Eur. J. 14 (2008) 1718.
[43] V.M. Martinez, G. De Cremer, M.B.J. Roeffaers, M. Sliwa, M. Baruah, D.E. De Vos, J. Hofkens, B.F. Sels, J. Am. Chem. Soc. 130 (2008) 13192.
[44] M.B.J. Roeffaers, G. De Cremer, H. Uji-i, B. Muls, B.F. Sels, P.A. Jacobs, F.C. De Schryver, D.E. De Vos, J. Hofkens, Proc. Natl. Acad. Sci. U.S.A. 104 (2007) 12603.
[45] B.M. Weckhuysen, Angew. Chem., Int. Ed. 48 (2009) 4910.
[46] M.B.J. Roeffaers, B.F. Sels, H. Uji-i, B. Blanpain, P. L'Hoest, P.A. Jacobs, F.C. De Schryver, J. Hofkens, D.E. De Vos, Angew. Chem., Int. Ed. 46 (2007) 1706.
[47] E. Stavitski, M.H.F. Kox, B.M. Weckhuysen, Chem. Eur. J. 13 (2007) 7057.
[48] H.C. Kang, R.P. Haugland, Ethenyl-substituted dipyrrometheneboron difluoride dyes and their synthesis, Molecular Probes, Inc., Eugene, OR, US Patent 005187288A (1993).
[49] G. De Cremer, M.B.J. Roeffaers, E. Bartholomeeusen, K. Lin, D. Dedecker, P.P. Pescarmona, P.A. Jacobs, D.E. De Vos, J. Hofkens, B.F. Sels, Angew. Chem., Int. Ed. 49 (2010) 908.
[50] P.O. Gendron, F. Avaltroni, K.J. Wilkinson, J. Fluoresc. 18 (2008) 1093.
[51] B. Huang, W.Q. Wang, M. Bates, X.W. Zhuang, Science 319 (2008) 810.